Acousto-optic pulse picking scheme with carrier-frequency-to-pulse-repetition-rate synchronization

Oliver de Vries,[1,*] Tobias Saule,[2] Marco Plötner,[1] Fabian Lücking,[3] Tino Eidam,[4,5,6] Armin Hoffmann,[4] Arno Klenke,[4,5] Steffen Hädrich,[4,5] Jens Limpert,[4,5,6] Simon Holzberger,[2] Thomas Schreiber,[1] Ramona Eberhardt,[1] Ioachim Pupeza,[2] and Andreas Tünnermann[1,4]

[1]*Fraunhofer Institute for Applied Optics and Precision Engineering, Albert-Einstein-Str. 7, 07745 Jena, Germany*
[2]*Max-Planck-Institut für Quantenoptik, Hans-Kopfermann-Straße 1, 85748 Garching, Germany*
[3]*Femtolasers Produktions GmbH, Fernkorngasse 10, 1100 Vienna, Austria*
[4]*Institute of Applied Physics, Abbe Center of Photonics, Friedrich-Schiller-Universität Jena, Albert-Einstein-Str. 15, 07745 Jena, Germany*
[5]*Helmholtz-Institute Jena, Fröbelstieg 3, 07743 Jena, Germany*
[6]*Active Fiber Systems GmbH, Wildenbruchstr. 15, 07745 Jena, Germany*
[*]*oliver.devries@iof.fraunhofer.de*

Abstract: We introduce and experimentally validate a pulse picking technique based on a travelling-wave-type acousto-optic modulator (AOM) having the AOM carrier frequency synchronized to the repetition rate of the original pulse train. As a consequence, the phase noise characteristic of the original pulse train is largely preserved, rendering this technique suitable for applications requiring carrier-envelope phase stabilization. In a proof-of-principle experiment, the 1030-nm spectral part of an 74-MHz, carrier-envelope phase stable Ti:sapphire oscillator is amplified and reduced in pulse repetition frequency by a factor of two, maintaining an unprecedentedly low carrier-envelope phase noise spectral density of below 68 mrad. Furthermore, a comparative analysis reveals that the pulse-picking-induced additional amplitude noise is minimized, when the AOM is operated under synchronicity. The proposed scheme is particularly suitable when the down-picked repetition rate is still in the multi-MHz-range, where Pockels cells cannot be applied due to piezoelectric ringing.

OCIS codes: (250.4110) Modulators; (140.3538) Lasers, pulsed; (140.3425) Laser stabilization.

References and links

1. P. Russbueldt, T. Mans, J. Weitenberg, H. D. Hoffmann, and R. Poprawe, "Compact diode-pumped 1.1 kW Yb:YAG Innoslab femtosecond amplifier," Opt. Lett. **35**(24), 4169–4171 (2010).
2. T. Eidam, S. Hanf, E. Seise, T. V. Andersen, T. Gabler, C. Wirth, T. Schreiber, J. Limpert, and A. Tünnermann, "Femtosecond fiber CPA system emitting 830 W average output power," Opt. Lett. **35**(2), 94–96 (2010).
3. M. Pittman, S. Ferré, J. P. Rousseau, L. Notebaert, J. P. Chambaret, and G. Chériaux, "Design and characterization of a near-diffraction-limited femtosecond 100-TW 10-Hz high-intensity laser system," Appl. Phys. B **74**(6), 529–535 (2002).
4. T. Metzger, A. Schwarz, C. Y. Teisset, D. Sutter, A. Killi, R. Kienberger, and F. Krausz, "High-repetition-rate picosecond pump laser based on a Yb:YAG disk amplifier for optical parametric amplification," Opt. Lett. **34**(14), 2123–2125 (2009).
5. T. Eidam, J. Rothhardt, F. Stutzki, F. Jansen, S. Hädrich, H. Carstens, C. Jauregui, J. Limpert, and A. Tünnermann, "Fiber chirped-pulse amplification system emitting 3.8 GW peak power," Opt. Express **19**(1), 255–260 (2011).
6. I. Pupeza, S. Holzberger, T. Eidam, H. Carstens, D. Esser, J. Weitenberg, P. Rußbüldt, J. Rauschenberger, J. Limpert, T. Udem, A. Tünnermann, T. W. Hänsch, A. Apolonski, F. Krausz, and E. Fill, "Compact high-repetition-rate source of coherent 100 eV radiation," Nat. Photonics **7**(8), 608–612 (2013).
7. A. Cingöz, D. C. Yost, T. K. Allison, A. Ruehl, M. E. Fermann, I. Hartl, and J. Ye, "Direct frequency comb spectroscopy in the extreme ultraviolet," Nature **482**(7383), 68–71 (2012).

#241120 Received 18 May 2015; revised 13 Jul 2015; accepted 16 Jul 2015; published 20 Jul 2015

8. S. Hädrich, A. Klenke, J. Rothhardt, M. Krebs, A. Hoffmann, O. Pronin, V. Pervak, J. Limpert, and A. Tünnermann, "High photon flux table-top coherent extreme ultraviolet source," Nat. Photonics **8**(10), 779–783 (2014).
9. Z. Huang and R. Ruth, "Laser-Electron Storage Ring," Phys. Rev. Lett. **80**(5), 976–979 (1998).
10. V. Malka, J. Faure, Y. A. Gauduel, E. Lefebvre, A. Rousse, and K. T. Phuoc, "Principles and applications of compact laser–plasma accelerators," Nat. Phys. **4**(6), 447–453 (2008).
11. J. Rothhardt, S. Demmler, S. Hädrich, J. Limpert, and A. Tünnermann, "Octave-spanning OPCPA system delivering CEP-stable few-cycle pulses and 22 W of average power at 1 MHz repetition rate," Opt. Express **20**(10), 10870–10878 (2012).
12. A. Baltuška, T. Fuji, and T. Kobayashi, "Controlling the Carrier-Envelope Phase of Ultrashort Light Pulses with Optical Parametric Amplifiers," Phys. Rev. Lett. **88**(13), 133901 (2002).
13. G. D. Goodno, Z. Guo, R. J. D. Miller, I. J. Miller, J. W. Montgomery, S. R. Adhav, and R. S. Adhav, "Investigation of β-BaB2O4 as a Q-switch for high power applications," Appl. Phys. Lett. **66**(13), 1575–1577 (1995).
14. N. Uchida and N. Niizeki, "Acoustooptic deflection materials and techniques," Proc. IEEE **61**(8), 1073–1092 (1973).
15. S. Koke, C. Grebing, H. Frei, A. Anderson, A. Assion, and G. Steinmeyer, "Direct frequency comb synthesis with arbitrary offset and shot-noise-limited phase noise," Nat. Photonics **4**(7), 462–465 (2010).
16. B. Borchers, F. Lücking, and G. Steinmeyer, "Acoustic frequency combs for carrier-envelope phase stabilization," Opt. Lett. **39**(3), 544–547 (2014).
17. W. J. Schwenger and J. M. Higbie, "High-speed acousto-optic shutter with no optical frequency shift," Rev. Sci. Instrum. **83**(8), 083110 (2012).
18. T. M. Fortier, D. J. Jones, J. Ye, S. T. Cundiff, and R. S. Windeler, "Long-term carrier-envelope phase coherence," Opt. Lett. **27**(16), 1436–1438 (2002).
19. F. Lücking, A. Assion, A. Apolonski, F. Krausz, and G. Steinmeyer, "Long-term carrier-envelope-phase-stable few-cycle pulses by use of the feed-forward method," Opt. Lett. **37**(11), 2076–2078 (2012).
20. K. F. Mak, M. Seidel, O. Pronin, M. H. Frosz, A. Abdolvand, V. Pervak, A. Apolonski, F. Krausz, J. C. Travers, and P. S. J. Russell, "Compressing μJ-level pulses from 250 fs to sub-10 fs at 38-MHz repetition rate using two gas-filled hollow-core photonic crystal fiber stages," Opt. Lett. **40**(7), 1238 (2015).
21. J. Rothhardt, S. Hädrich, A. Klenke, S. Demmler, A. Hoffmann, T. Gotschall, T. Eidam, M. Krebs, J. Limpert, and A. Tünnermann, "53 W average power few-cycle fiber laser system generating soft x rays up to the water window," Opt. Lett. **39**(17), 5224–5227 (2014).
22. M. I. Stockman, M. F. Kling, U. Kleineberg, and F. Krausz, "Attosecond nanoplasmonic-field microscope," Nat. Photonics **1**(9), 539–544 (2007).

1. Introduction

Mode-locked laser oscillators used as seeding sources for high-power amplifier systems often emit at tens of MHz pulse repetition frequencies, eventually leading to moderate pulse energies after amplification. Nowadays femtosecond amplifier systems operating at 1-μm wavelength reach kW-level average powers with close-to diffraction limited beam quality. However, since the repetition rate is on the order of tens of MHz, the peak power will still be limited to some megawatts [1,2]. Increasing the pulse energy and the peak power without the compelling necessity of a simultaneously scaled average power by successive down-picking of the pulse repetition frequency between the amplifier stages is an established method [3–5]. Such high-peak and high-average power laser systems are ideal tools for many applications in science, medicine and industry, including high-harmonic generation [6–8], coherent gamma-ray generation [9] or laser wakefield acceleration [10]. Along with the requirements of high average and peak power, typically all these applications demand high pulse amplitude stability and, sometimes, carrier-envelope (CE) phase control as well.

Reducing high pulse repetition rates requires switching methods that periodically pick single pulses out of an input pulse train. This can be done optically by selectively amplifying single pulses in nonlinear crystals [11], an approach which even preserves CE phase stability [12]. However, since this represents an optically complex procedure, it is only reasonable if optical parametric amplification is intended from the start. Well-established and more convenient electronical switching techniques employ Pockels cells and acousto-optic modulators. Depending on crystal material, electrode arrangement and geometrical dimensions, Pockels cells are typically driven with kV-level voltages. The analysis of specifications provided by different manufacturers using different electro-optic materials reveal nominal half-wave voltages reaching from approximately 0.5–3 kV per millimeter of

#241120 Received 18 May 2015; revised 13 Jul 2015; accepted 16 Jul 2015; published 20 Jul 2015

clear aperture. Realized as high-speed switches for multi-MHz pulse repetition frequencies, expensive power electronics with slew rates of hundreds of volt per nanosecond are necessary. Additionally, the output repetition frequency is limited to some hundreds of kHz due to piezoelectric ringing in the commonly used crystals ($LiNbO_3$, BBO, RTP etc.) [13]. Low-power integrated electro-optic modulators can switch very rapidly but, in comparison to Pockels cells, they suffer from higher insertion losses and a less pronounced contrast. Acousto-optic modulators (AOMs) [14] made of e.g. tellurium dioxide with low operating voltage are commercially available with nominal carrier frequencies of some hundreds of MHz, rendering them as either a suitable alternative for fast pulse picking applications or, if the down-picked repetition frequency remains well above MHz-level, as the means of choice.

Although the AOM pulse picking approach has numerous benefits, it exhibits two major drawbacks. First, for reaching high contrast between picked and blocked pulses, usually the 1st Bragg diffraction order is used as output for the down-picked pulse train. Therefore, a travelling-wave-type AOM imposes a Doppler-frequency shift equal to the AOM carrier frequency on the optical comb of the picked pulses and, thus, creating (or contributing to) a new carrier-envelope-offset frequency. This very effect can be exploited to provide CE phase stabilization to a free-running mode-locked laser [15], but in this case the AOM is not used as pulse picker. Pulse picking can in principle be combined with stabilization, but was only demonstrated for bursts of pulses with picking frequencies below the kHz range [16]. Second, as we will show in detail later on, if the AOM carrier signal has no defined phase relation with the gating signal, the down-picked output pulses will be prone to peak power fluctuations due to diffraction efficiency variations. It should be noted that standing-wave-type or frequency-shift-compensating AOMs do not suffer from these drawbacks but are still subject to research and are not yet suitable for gating times below 25 ns [17]. Using travelling-wave-type AOMs in zero-diffraction-order configuration would also circumvent both issues but, inherent to this scheme, provides insufficient suppression of the blocked pulses.

In this paper we introduce a technique enabling a travelling-wave-type AOM (used in 1st diffraction order) to be utilized for the reduction of the pulse repetition frequency of a CE phase stable femtosecond pulse train with a CE phase noise characteristic close to that of the starting oscillator. By mixing two electronic RF signals (square-wave gating and sinusoidal AOM carrier), both derived from the pulse repetition frequency of the laser oscillator, the AOM-imposed frequency shift does not alter the value of the CE offset frequency and, thus, CE phase stability is maintained. A constant phase relation between gating and AOM carrier also ensures low additional pulse-to-pulse amplitude fluctuations of the picked pulses, since deviations of AOM diffraction efficiency are avoided as compared to using an arbitrary AOM carrier frequency. To the best of our knowledge, this issue was never explicitly addressed before.

To experimentally validate phase and amplitude stability, the proposed pulse picking scheme is implemented in an Yb-doped fiber amplifier configuration. To this end, the long-wavelength spectral part (>1020 nm) of a CE phase stabilized 73.8-MHz repetition rate Ti:sapphire mode-locked laser is amplified and reduced in its repetition frequency by a factor of two. Comparative experiments reveal additional amplitude noise when the AOM carrier signal is not synchronized to the pulse repetition frequency (standard approach) showing that not only CE phase stable systems benefit from our findings, but rather any pulsed laser system relying on acousto-optic reduction of the pulse repetition frequency.

2. Theory

In case of a continuously driven AOM (i.e., no pulse picking), the spectral lines of the input optical frequency comb are defined as [18]

$$f_m = m f_{\mathrm{REP}} + f_{\mathrm{CEO}}, \tag{1}$$

#241120 Received 18 May 2015; revised 13 Jul 2015; accepted 16 Jul 2015; published 20 Jul 2015

with an integer m, the input pulse repetition frequency f_{REP} and the CE offset frequency f_{CEO}. When a travelling-wave-type AOM is utilized, usually the plus/minus 1st Bragg diffraction order is used to benefit from the high transmittance contrast between on- and off-state. The comb in the diffracted beam will then be Doppler-shifted by the value of the AOM carrier frequency

$$f_m = m f_{\mathrm{REP}} + \left(f_{\mathrm{CEO}} \pm f_{RF}\right). \tag{2}$$

If the same AOM is used for pulse picking, an AOM carrier frequency can be chosen, fulfilling what we call the synchronicity condition

$$f_{\mathrm{RF}} = \frac{u}{p} f_{\mathrm{REP}}, \tag{3}$$

with an integer number u and the (integer) pulse picking factor p. If this condition is met, the frequency comb from Eq. (2) becomes

$$f^*_m = \left(m \pm u\right) \frac{f_{\mathrm{REP}}}{p} + f_{\mathrm{CEO}} = \left(m \pm u\right) f^*_{\mathrm{REP}} + f_{\mathrm{CEO}}. \tag{4}$$

After the pulse picking process a new (reduced) output pulse repetition frequency f^*_{REP} is created, generating also a new (narrower) frequency comb with spacing $f^*_{\mathrm{REP}} = f_{\mathrm{REP}}/p$. Additionally, the new comb in Eq. (4) is shifted by plus / minus u lines but is maintaining the original f_{CEO}. For preservation of CE phase stability, it is essential that f_{CEO} will not be altered during the pulse picking process.

The newly generated CE offset phase can now be defined as

$$\Delta\phi^*_{\mathrm{CEO}} = 2\pi \frac{f_{\mathrm{CEO}}}{f^*_{\mathrm{REP}}}, \mathrm{mod}\, 2\pi. \tag{5}$$

For $f_{\mathrm{CEO}} = 0$ this means that there will be no pulse-to-pulse phase slip or, in other words, the CE offset phase will remain at $\Delta\phi^*_{\mathrm{CEO}} = 0$. But in the case, where f_{CEO} is the a -th fraction of the pulse repetition frequency $f_{\mathrm{CEO}} = f_{\mathrm{REP}}/a$, the CE offset phase in Eq. (5) becomes

$$\Delta\phi^*_{\mathrm{CEO}} = 2\pi \frac{p}{a}, \mathrm{mod}\, 2\pi. \tag{6}$$

Thus, if the ratio p/a takes an integer value, the pulse-to-pulse phase slip is effectively cancelled out.

Regarding the synchronicity condition from Eq. (3), with a given pulse picking factor p the best choice for the integer u is when the AOM carrier frequency f_{RF} becomes close to the AOM nominal carrier frequency $f_{\mathrm{RF\_NOM}}$. This ensures a sound functionality of the AOM transducer electronics and in case of fiber-coupled AOMs an optimum coupling due to the mutual dependence between AOM carrier frequency, angle of incidence and diffraction efficiency [14]. Maybe the most elegant interpretation of Eq. (3) is to choose the AOM carrier frequency as an integer multiple of the pulse repetition frequency $f_{\mathrm{RF}} = n f_{\mathrm{REP}}$, which perforce fulfills the synchronicity condition and, most importantly, it does so independently of the pulse picking factor p.

#241120 Received 18 May 2015; revised 13 Jul 2015; accepted 16 Jul 2015; published 20 Jul 2015

The origin of the AOM-induced pulse amplitude noise is illustrated in Fig. 1, which shows the basic principle of generating the electronic AOM driver signal leading to pulse peak power fluctuations. The gating signal (timed to the input pulse train) with frequency $f^*_{\mathrm{REP}} = f_{\mathrm{REP}}/p$ and the AOM carrier signal with a frequency f_{RF} are mixed to produce the pulse picking AOM driver signal. Typically, a local RF oscillator is generating the AOM carrier frequency f_{RF} with no correlation to either the laser oscillator pulse repetition frequency f_{REP}, or the gating signal frequency. This results in a phase difference $\Delta\phi$ between two adjacent acoustic compression wave packets. This phase difference effectively causes a diffraction efficiency modulation and, therefore, an amplitude modulation of the picked output pulse train. This becomes particularly pronounced when pulses are picked from a high-repetition-rate pulse train, where the gating signal has to be extremely short with just a few cycles left for the AOM carrier signal to generate a moving acoustic compression wave at the piezo-electric transducer. Due to the relatively slow speed of sound in the AOM medium (e.g. 4250 ms^{-1} for TeO_2), these travelling acoustic compression wave packets are as short as just a few tens of µm, explaining the need for small beam waists.

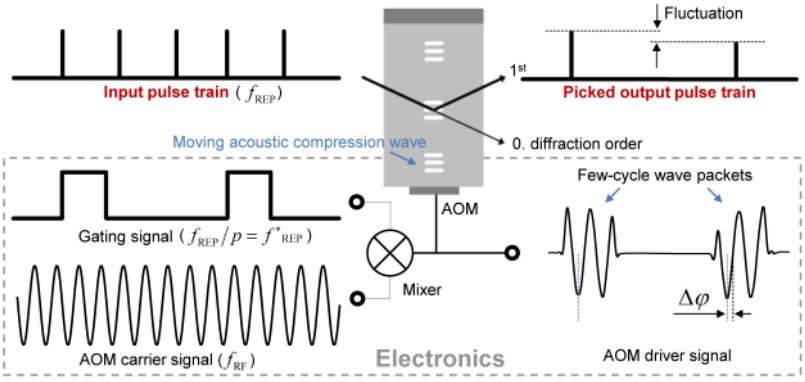

Fig. 1. Schematic setup of the AOM pulse picking electronics showing the origin of pulse peak power fluctuations caused by a non-synchronized AOM carrier signal (AOM, acousto-optic modulator; $\Delta\varphi$, phase difference between two adjacent wave packets).

Whichever AOM parameters are aimed for, the pulse peak power fluctuations would be efficiently reduced if $\Delta\varphi$ became zero. Exactly this happens if (a) the gating frequency equals $f^*_{\mathrm{REP}} = f_{\mathrm{REP}}/p$ and (b) the synchronicity condition for the AOM carrier frequency f_{RF} in Eq. (3) is fulfilled. Assuming there is a unique diffraction efficiency for each phase position of the acoustic compression wave packet, any deviation of f_{RF} from the synchronicity condition will generate a difference frequency

$$\Delta f_{\mathrm{RF}} = f_{\mathrm{RF}} - \frac{u}{p} f_{\mathrm{REP}}, \tag{7}$$

which represents an asynchronicity that consistently leads to a non-zero phase difference

$$\Delta\varphi = \left(2\pi\, f_{\mathrm{RF}}\, \Delta t\right) - \left(2\pi \frac{u}{p} f_{\mathrm{REP}}\, \Delta t\right) = 2\pi \left(p \frac{\Delta f_{\mathrm{RF}}}{f_{\mathrm{REP}}}\right) \bmod 2\pi, \tag{8}$$

with $\Delta t = f^{*}_{\mathrm{REP}}{}^{-1} = p/f_{\mathrm{REP}}$. As it will be shown in Section 3, the difference frequency Δf_{RF} can be seen as an amplitude modulation in the RF spectrum when analyzing the pulse train.

#241120 Received 18 May 2015; revised 13 Jul 2015; accepted 16 Jul 2015; published 20 Jul 2015

To summarize the basic idea of this work, two major drawbacks related to travelling-wave-type AOM-based pulse picking, namely loss of CE phase stability and added pulse amplitude noise, can be overcome by choosing an f_{REP}-synchronized condition for the AOM carrier frequency f_{RF} as stated in Eq. (3).

3. Experimental setting

To experimentally verify the main statements of the argument described above, an experiment was set up as schematically shown in Fig. 2.

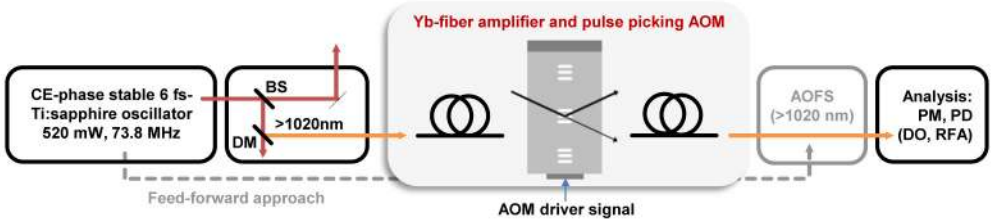

Fig. 2. Schematic experimental setup of the Yb-doped fiber amplifier with implemented AOM pulse picking scheme (PM, power meter; PD, photodiode; DO, digital oscilloscope; RFA, radio frequency analyzer; BS, beam splitter; DM, dichroic mirror; AOFS, acousto-optic frequency shifter; AOM, acousto-optic modulator).

The initial f_{REP} = 73.8-MHz repetition frequency train of 6-fs pulses with an average power of 520 mW was generated by a commercially available Ti:sapphire oscillator (rainbow CEP4, Femtolasers). The system is equipped with a feed-forward type CE phase stabilization unit ($f_{\mathrm{CEO}} = 0$) realized by an acousto-optic frequency shifter (AOFS) [19]. The >1020-nm part of the emitted spectrum (200 µW of average power, 3.4 pJ of pulse energy) is used to seed a multi-stage Yb-doped fiber amplifier system, including a travelling-wave-type pulse picking AOM with a nominal carrier frequency of $f_{\mathrm{RF\_NOM}}$ = 230 MHz. For demonstration purposes, a pulse picking factor of $p = 2$ was chosen, resulting in an overall amplification factor of 450 (for the average power) and 900 (for the pulse energy), generating a 3.1-nJ pulse train with >110 mW of output power. By using the AOM −1st diffraction order for the picked pulses, an inherently high suppression of the blocked pulses was observed by analyzing the time trace with a fast photodiode (rise time <70 ps). Taking into account the 8-bit limited dynamic range of the digital oscilloscope, the measurement of pulse peak to noise floor level revealed no residual pulses in between the down-picked pulse train indicating a suppression of the blocked pulses of >20 dB.

According to Eq. (3), the synchronicity condition for the AOM carrier frequency is reached for $f_{\mathrm{RF}} = 221.45$ MHz, which is three times f_{REP} (with $u = 6$). Since every second pulse is blocked, a gating duty cycle of ~50 percent was chosen, resulting in a gating time of ~13 ns. With this gate width, and the stated carrier frequency, an acoustic compression wave packet consists of less than three AOM carrier cycles, making this particular setting especially prone to causing peak power fluctuations as long as no synchronization is utilized.

3.1 CE phase stability

In a first experiment, the CE phase stability was investigated after the f_{REP}-synchronized AOM carrier frequency was applied to the pulse picking process. In the case at hand, a direct measurement of the CE phase noise spectral density with an f-2f-interferometer was not possible, since the spectral bandwidth of the amplified pulse train was only about 10 nm around 1030 nm and the pulse peak power was not yet high enough for spectral broadening

#241120 Received 18 May 2015; revised 13 Jul 2015; accepted 16 Jul 2015; published 20 Jul 2015

and frequency doubling. For these reasons an indirect method to evaluate CE phase stability was carried out, as schematically shown in Fig. 3.

Both arms of the split oscillator output were CE phase stabilized using two AOFS: one for the >1020-nm signal arm as also depicted in Fig. 2, and another for the almost octave-spanning spectrum around 800 nm. By means of a matched delay line, the CE phase-stable pulses of the 800-nm and 1030-nm signal arms were spatially and temporally overlapped on a fast photodiode.

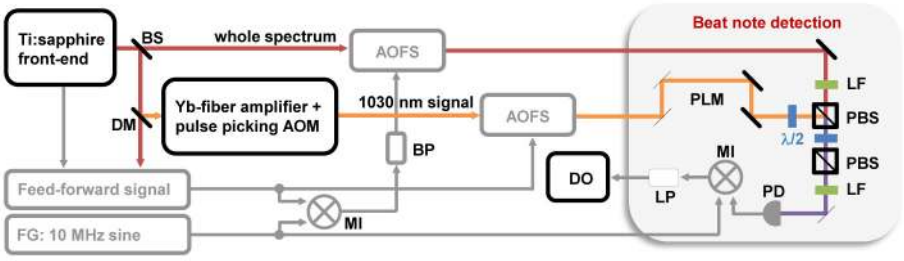

Fig. 3. Schematic experimental setup of the beat note detection for CE phase noise measurement (PLM, path-length matching; DM, dichroic mirror; BS, beam splitter; LF, optical long-wave pass filter (>1020 nm); PBS, polarization beam splitter; PD, photodiode; FG, function generator; MI, electronical mixer; BP, band pass filter ($f_{REP} - 10$ MHz); LP, low-pass filter (1.9 MHz); AOFS, acousto-optic frequency shifter; DO, digital oscilloscope).

To enable a frequency-resolved measurement, the signal was shifted out of the baseband by a 10-MHz detuning of the 800-nm AOFS carrier frequency. To directly extract the phase noise out of the beat note detection, the measured photodiode signal was mixed with the 10-MHz signal used for detuning, low-pass filtered at 1.9 MHz and sampled with a digital oscilloscope. The (one-sided) power spectral density (PSD) and the integrated PSD of this signal were calculated and plotted in Fig. 4.

This measurement shows the phase noise jitter of the relative optical frequencies of the two combs caused by the pulse picking scheme, by amplification and by the delay stage. The integrated PSD of <25 mrad for frequencies from 1 kHz to 500 kHz marks the upper limit to this added noise as it includes the noise floor of our detection setup itself.

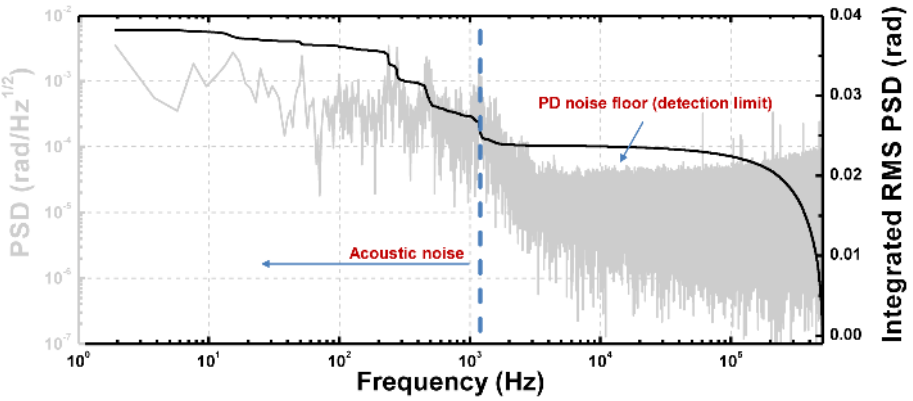

Fig. 4. Noise spectral density (grey) and integrated phase noise (black) extracted from the beat note between the 800-nm and the 1030-nm signal arm. Frequency components <1 kHz correspond to mechanical and acoustic noise, high-frequency noise is mainly due to the detection limit (PSD, power spectral density; RMS, root mean square).

Noise contributions below 1 kHz stem predominantly from mechanical vibrations and acoustic noise, since no measures have been taken to actively stabilize the interferometer. In

#241120 Received 18 May 2015; revised 13 Jul 2015; accepted 16 Jul 2015; published 20 Jul 2015

the full range of the measurement (2 Hz–500 kHz) the integrated PSD stays below 38 mrad. The integrated noise level of the oscillator CE phase stabilization is known (<25 mrad for 1 kHz–500 kHz, <30 mrad total [19]), allowing us to estimate the overall CE phase stability of the system. In the worst case of fully correlated noise, the three noise sources – oscillator, pulse picking scheme, and amplifier – add up to a total integrated PSD of 48 mrad between 1 kHz and 500 kHz and 68 mrad for the full range. In contrast, quasi-random phase differences from shot to shot were observed when a non-synchronized drive frequency was applied to the pulse picker.

This clearly proves that the synchronized AOM pulse picking approach can be applied even to CE phase-stable pulse trains with a minimum impact on residual phase noise. Notably, it represents the lowest phase jitter value ever achieved with a 1030-nm front-end with average output powers >100 mW. This constitutes an important step towards high-power applications, where stable pulse-to-pulse coherence is mandatory [20].

3.2 Amplitude stability

In a second experiment, the influence on the pulse amplitude stability when using a synchronized ($\Delta f_{RF} = 0$) in comparison to a non-synchronized AOM carrier ($\Delta f_{RF} \neq 0$) was investigated. Different non-synchronized AOM carrier signals with offset frequencies Δf_{RF} reaching from 50 kHz to 20 MHz were compared with the synchronized carrier. All detunings yielded similar results, but for the sake of clarity, the comparison with $\Delta f_{RF} = 2$ MHz ($f_{RF} = 223.45$ MHz) will be representatively discussed in detail. Due to current limitations on the part of the AOM electronics, the power of the AOM driver signal is at 50 percent nominal level, where the diffraction efficiency response is most sensitive to the phasing between the gating and carrier signals, constituting an unfavorable pulse picking regime. This clearly demonstrates the impact of diffraction efficiency variations through $\Delta\varphi \neq 0$ [(Eq. (8)] and pronounces the appearance of amplitude modulation sidebands in the RF spectrum. However, pulse amplitude fluctuations, albeit smaller, can be observed in nearly every AOM pulse picking scheme.

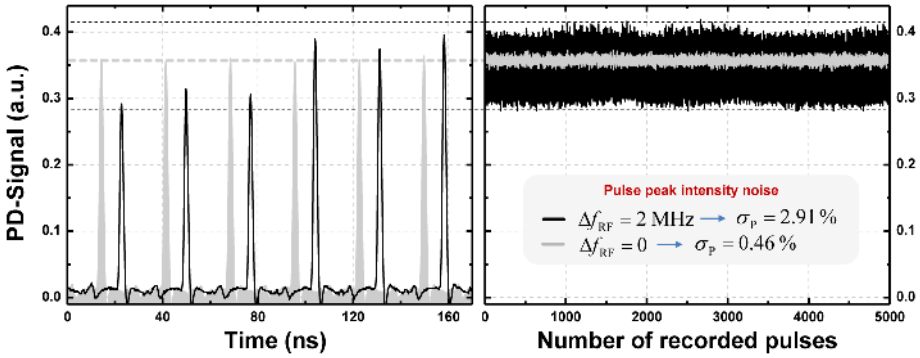

Fig. 5. Left side: Zoom on photodiode signal of picked pulse train using a synchronized (grey) versus a non-synchronized (black) AOM carrier frequency in a phasing-sensitive AOM regime. Right side: Analysis of 5000 adjacent pulse peak intensities showing a significant reduction of the standard deviation when using a synchronized AOM carrier.

To quantify the amplitude fluctuations, the individual peak heights of altogether 5000 pulses were determined by digitalizing the photodiode signal. The standard deviation σ_P as a measure of pulse peak intensity noise could thus be calculated. The results of the photodiode analysis is shown in Fig. 5. On the left, the time-trace directly shows the positive impact on the pulse amplitude stability of a synchronized AOM carrier (filled grey) as compared to a

#241120 Received 18 May 2015; revised 13 Jul 2015; accepted 16 Jul 2015; published 20 Jul 2015

detuned AOM carrier with $\Delta f_{RF} = 2$ MHz . On the right, the analysis of 5000 recorded pulses reveals peak intensity fluctuations within a 135-µs time span.

The respective standard deviation of the pulse amplitude in a pulse picking setup with synchronized AOM carrier was, in our setting, reduced by a factor of more than six compared to the non-synchronized case. Note that the measured standard deviation of 0.46 percent in the synchronized case is likely limited by the measurement precision. With a dwell time of 200 ps and a pulse full-width-at-half-maximum duration of 1.8 ns, the exact pulse peak intensities can be ascertained only with a limited accuracy.

As can be seen in Fig. 6 (left, black line), deviations of the AOM carrier frequency from the synchronicity condition result in sidebands around the reduced pulse repetition frequency in the RF spectrum of the photodiode signal. The reason can be traced back to the measured AOM driver signal [Fig. 6, right-hand side], which reveals a change in the pulse-to-pulse wave packet phase according to Eq. (8) of $\Delta\varphi = 0,34$ rad , resulting in a continuous change of the AOM diffraction efficiency and eventually of the pulse peak power. In contrast, the synchronized AOM driver signal generates no phase difference between two adjacent wave packets ($\Delta\varphi = 0$), and consequently no sidebands appear in the RF spectrum [Fig. 6, grey lines].

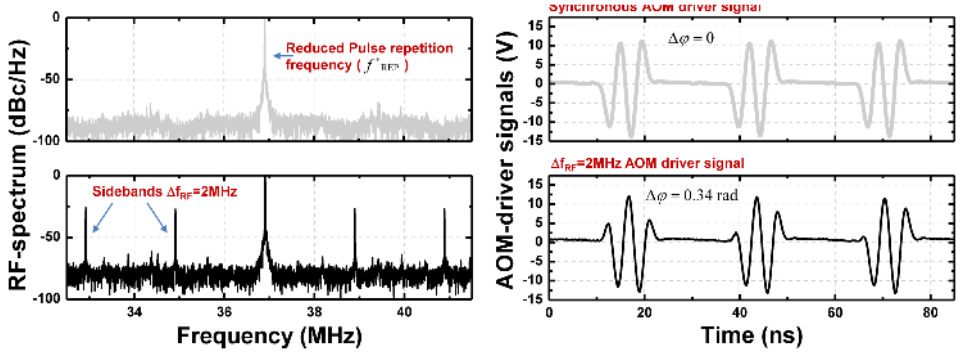

Fig. 6. Left side: RF spectra around the factor $p = 2$ reduced pulse repetition frequency at ~37 MHz. The 2-MHz sidebands disappear when a synchronized AOM carrier is used (grey). Right side: Measured AOM driver signals comparing non-synchronized (black) and synchronized (grey) AOM carrier when mixed with the gating signal.

These results should be understood as exemplary, as the degree of improvement in pulse peak intensity noise is strongly dependent on the AOM setting and cannot be generalized. In terms of amplitude stability, even an electronically optimized AOM pulse picking setup (not only for CE phase-stable but for any pulsed laser) will benefit to some extent from the proposed f_{REP} -synchronized AOM carrier scheme.

Finally, it should be noted that $\Delta\varphi = 0$ could, in principle, also be attained when a pre-programmed short wave packet would be synthesized electronically each time the AOM gating signal is triggered. For sufficiently high timing precision of the underlying synthesizer, this is equivalent to a phase-coherent RF scheme as described above. However, this alternative approach was not tested so far.

4. Conclusion

We have introduced and demonstrated a technique utilizing a travelling-wave-type AOM in a high-contrast, high-repetition-rate pulse picking scheme, where pulse peak power fluctuations have to be kept at a minimum. This method can even be used to reduce the pulse repetition frequency of CE phase-stable pulse trains. By using a gating signal and an AOM carrier synchronized to the pulse repetition frequency, the pulse peak intensity noise can be reduced

#241120 Received 18 May 2015; revised 13 Jul 2015; accepted 16 Jul 2015; published 20 Jul 2015

significantly compared to a setting with a freely chosen, non-synchronized AOM driver signal. The difference between synchronized and non-synchronized AOM carrier frequencies can directly be observed in the RF spectrum of the picked pulse train as clearly distinguishable amplitude modulations, adding new lines to the comb.

In a proof-of-principle experiment we amplified and at the same time reduced the pulse repetition frequency of the 1030-nm spectral part of an almost octave-spanning Ti:sapphire femtosecond oscillator equipped with a low-noise feed-forward CE phase stabilization system. A pulse train with an average output power exceeding 100 mW (gain factor 450) and 3.1-nJ pulses (gain factor 900) was generated, while the integrated CE phase noise PSD remained as low as 68 mrad (2 Hz–500 kHz) and 48 mrad (1 kHz–500 kHz), respectively.

The advantage of the proposed pulse picking technique via synchronized AOM carrier frequency becomes obvious, when subsequent applications demand CE phase stable, down-picked pulse trains in the multi-MHz range. In this case, Pockels cells cannot be applied due to limiting piezoelectric ringing effects and alternative techniques, like optical switching, might be beyond the scope of most experiments.

The setup demonstrated here constitutes a one-of-a-kind front-end for high-repetition-rate field-sensitive pump-probe experiments. Most prominently, the 1030-nm CE phase-stable output can be readily amplified using Yb-based power amplifiers to the power level necessary for efficient time compression via nonlinear spectral broadening and subsequent generation of high harmonics [6,8,20,21]. In this manner, the phase-stable generation of attosecond pulse trains and even of isolated attosecond pulses at multi-MHz repetition rates comes within reach. Together with the availability of the inherently synchronized and CE phase-stable few-cycle pulses from the 800-nm oscillator output, this paves the way to time-resolved photoelectron emission microscopy and spectroscopy experiments [22]. The adjustability of the repetition rate via pulse picking is a necessary prerequisite for avoiding the ambiguity of time-of-flight detection in these experiments.

Acknowledgments

This work was supported by the Fraunhofer and Max Planck cooperation program within the project “MEGAS”. A. K. acknowledges financial support by the Helmholtz-Institute Jena. T. E. acknowledges financial support by the Carl-Zeiss Stiftung. I. P. acknowledges funding by the European Research Council under the grant agreement no. [617173] “ACOPS”.

#241120 Received 18 May 2015; revised 13 Jul 2015; accepted 16 Jul 2015; published 20 Jul 2015